Journal of Solid State Chemistry **165,** 278–288 (2002)
doi:10.1006/jssc.2001.9521, available online at http://www/idealibrary.com on IDEAL®

High-Temperature Phase Transition in the Whitlockite-Type Phosphate $Ca_9In(PO_4)_7$

V. A. Morozov,*,† A. A. Belik,* S. Yu. Stefanovich,* V. V. Grebenev,* O. I. Lebedev,†,[1] G. Van Tendeloo,† and B. I. Lazoryak*

*Department of Chemistry, Moscow State University, 119899 Moscow, Russia; and †EMAT, University of Antwerp (RUCA), Groenenborgerlaan 171, B-2020 Antwerp, Belgium

Received October 8, 2001; in revised form January 15, 2002; accepted January 25, 2002

The double phosphate $Ca_9In(PO_4)_7$ was obtained by solid-state reaction and was studied by room and high-temperature X-ray powder diffraction, electron diffraction, high-resolution electron microscopy, second-harmonic generation (SHG) technique, differential scanning calorimetry, dielectric and conductivity measurements. The β-$Ca_9In(PO_4)_7$ room-temperature phase is related to the mineral whitlockite and is similar to β-$Ca_3(PO_4)_2$. It has space group $R\bar{3}c$, with unit cell parameters: $a = 10.4008(1)$ Å, $c = 37.272(1)$ Å, $Z = 6$. The structure was refined by the Rietveld method ($R_{wp} = 4.69$, $R_I = 1.81$). A reversible first-order $\beta \leftrightarrow \beta'$ phase transition of the ferroelectric type with $T_c = 902$ K is revealed by SHG, differential scanning calorimetry and dielectric measurements. The centrosymmetric β'-$Ca_9In(PO_4)_7$ (973 K) has space group $R\bar{3}c$, $a = 10.4611(2)$ Å, $c = 37.874(1)$ Å ($R_{wp} = 4.27$, $R_I = 4.11$). Compared to the low-temperature β-$Ca_9In(PO_4)_7$ structure, β'-$Ca_9In(PO_4)_7$ can be described as an orientational disordering of the $P1O_4$ tetrahedra together with a calcium disordering on the $M3$ site. © 2002 Elsevier Science (USA)

Key Words: **phosphates; crystal structure; Rietveld method; phase transition; X-ray diffraction; electron microscopy; second-harmonic generation. dielectric properties.**

1. INTRODUCTION

Calcium phosphate $Ca_3(PO_4)_2$ and its variations have been extensively studied as bioceramic materials (1–3). Previous studies have shown that calcium phosphate at room temperature usually exists in two stable forms: α- and β-modifications. The phase transition $\alpha \leftrightarrow \beta$ in $Ca_3(PO_4)_2$ has been studied by many researchers. The $\alpha \leftrightarrow \beta$ transformation temperature is estimated at 1408 ± 5 K (4), however the exact temperature strongly depends on the type and the quantity of the impurities in the calcium phosphate (5–7). In addition to these stable modifications other forms of $Ca_3(PO_4)_2$ such as α′- (8, 9), α″- (10) and a high-pressure form (11) have been described. There is evidence of a low-temperature phase transition in β-$Ca_3(PO_4)_2$ and different compounds with a whitlockite-type structure (12–16).

For the moment, only the structures of α- and β-$Ca_3(PO_4)_2$ have been studied. α-$Ca_3(PO_4)_2$ (space group $P2_1/a$, $Z = 24$) has a distorted β-K_2SO_4-type structure (17, 18). Calcium cations fully occupy the 18 (4-*fold*) positions. β-$Ca_3(PO_4)_2$ (space group $R3c$, $Z = 21$) (19) is isostructural to the natural mineral whitlockite: $Ca_{18.19}Mg_{1.17}H_{1.62}(PO_4)_{14}$ (20). Ca^{2+} cations occupy five positions $M1$–$M5$; the $M1$–$M3$ (18-*fold*) and $M5$ (6-*fold*) positions are fully occupied whereas $M4$ (6-*fold*) is half-occupied by calcium cations, $M6$ (6-*fold*) is vacant.

Double phosphates $Ca_9R^{3+}(PO_4)_7$ (R^{3+} = Al, Fe, Cr, Ga, Sc, In) are also known to be based on the structure of β-$Ca_3(PO_4)_2$ (21) and show a large resemblance with the natural mineral whitlockite. We have singled out two groups of compounds with R^{3+} = Fe, Cr, Sc and R^{3+} = Al, Ga, In, which the unit-cell parameter "c" changes identically. A recent investigation of the structure of $Ca_9Fe(PO_4)_7$ (22) has shown that Fe^{3+} cations are located in the $M5$ sites of the β-$Ca_3(PO_4)_2$ - type structure. Calcium cations occupy the $M1$–$M3$ sites, while the $M4$ and $M6$ sites are vacant. The structure of the second group of compounds has not yet been studied.

Kustova *et al.* were the first to pay attention to changes in temperature of the IR- spectrum of Cr^{3+}-stabilized β-$Ca_3(PO_4)_2$ and related them to a new phase transition in this compound (23). We have recently discovered a high-temperature ferroelectric phase transition at 890 ± 10 K in $Ca_9Fe(PO_4)_7$ (24). This reversible first-order $\beta \leftrightarrow \beta'$ phase transition changes the crystal structure from polar ($R3c$) to centosymmetric ($R\bar{3}c$) and is accompanied by a change in orientation of half of the $P1O_4$ tetrahedra. HREM studies have shown that microdomains with $R3m$ (or $R3$)

[1]To whom correspondence should be addressed. Fax: +32-32180257. E-mail: lebedev@ruca.ua.ac.be.

0022-4596/02 $35.00

symmetry are invariably present inside the $R3c$ matrix. Two remarks have to be made: (1) these microdomains are an integral part of the whitlockite-type structure; (2) these microdomains result from a composition change as the Ca/Fe ratio significantly varies from one crystallite to another.

A similar high-temperature reversible phase transition has been found in solid solutions of $Ca_{10.5-x}Sr_x(PO_4)_7$ ($0 \le x \le 8$, $Z = 6$) (25). The temperature of the phase transition as well as the signal of the second harmonic generation (SHG) decreases with increasing strontium content. Solid solutions for a composition $6.5 \le x \le 8$ have a center of symmetry and do not show any phase transformation, however, the compositions with $0 \le x \le 6$ show a transition from a polar phase to a centrosymmetric one.

In this paper, we study the high-temperature phase transition in the whitlockite-type phosphate $Ca_9In(PO_4)_7$ as well as the crystal structure at room temperature (β-modification) and high temperature (β'-modification).

2. EXPERIMENTAL

The double phosphate $Ca_9In(PO_4)_7$ was prepared from a stoichiometric mixture of $Ca_2P_2O_7$, $CaCO_3$ and In_2O_3 by a ceramic technique in an Al_2O_3 crucible at 1273 K for 90 h in air. XRD patterns of the prepared compound coincide with the patterns described earlier (26) and do not contain reflections of foreign phases.

X-ray diffraction (XRD) patterns for the structure refinement were collected on a SIEMENS D500 powder diffractometer equipped with a BRAUN position-sensitive detector (Bragg–Brentano geometry; room temperature: a primary SiO_2 monochromator, Cu$K\alpha_1$ radiation, λ = 1.5406 Å; high-temperature: Cu$K\alpha$ radiation, Filter—Ni). The room temperature X-ray data were collected over the range from 10 to 110° in 2Θ with a step of 0.01°. High-temperature XRD patterns of $Ca_9In(PO_4)_7$ were obtained over the temperature range from 293 to 1273 K. The data were collected over the range from 20 to 70° in 2Θ for the lattice parameter determination and from 10–110° for the structural refinement with a step of 0.02°. The powdered sample was mixed with cellulose nitrate varnish and pasted on a Pt plate. The Pt plate was used as a sample heater.

Electron diffraction (ED) and high-resolution electron-microscopy (HREM) investigations were made on crushed $Ca_9In(PO_4)_7$ samples deposited on holey carbon grids. ED patterns in the temperature region from 293 to 1193 K were performed in a Philips CM20 equipped with a double-tilt heating holder. EDX spectra were obtained using a LINK-2000 attachment. HREM observations at room temperature were performed using a JEOL 4000 EX microscope operating at 400 kV. The Scherzer resolution of the microscope is 1.7 Å. Simulations of the HREM images were performed using the MacTampas software.

The second-harmonic generation response of powder samples was measured with a Q-switched YAG:Nd laser at λ_ω = 1.064 mcm, in the reflection mode. The experimental setup and arrangement have been described elsewhere (27). Differential scanning calorimetry (DSC) measurements were performed on a NETZSCH STA 409 difference-scanning calorimeter in the temperature region from 293 to 1013 K. The heating rate was 5 K/min.

In order to characterize the dielectric properties of $Ca_9In(PO_4)_7$, ceramic samples were prepared. Disk-like pellets were pressed-out of the $Ca_9In(PO_4)_7$ powder and then sintered at 1300 K during 2 h. Platinum paste was put on the surfaces of the disks and heated to produce metal electrodes. Measurements were performed of the dielectric constant (δ), the dielectric losses tangent (tan δ) and the specific electrical conductivity (σ) versus temperature with computer-controlled *ac*-bridges R5083 and E7-12 in the range of electric-field frequency between 10 kHz and 1 MHz in a temperature interval of 290–1200 K.

3. ROOM TEMPERATURE β-PHASE

3.1. Sample Composition (EDX)

The indium content in different crystallites of $Ca_9In(PO_4)_7$ was evaluated by quantitative EDX analysis performed inside the electron microscope. The ratio Ca/In (ideally equal to 9) for different crystallites remains practically constant and reveals a regular indium distribution in the sample.

3.2. X-Ray Structure Determination

We have analyzed the X-ray diffraction data by the Rietveld method (28) with RIETAN-2000 (29) on the basis of the space group $R3c$ (No. 161) using fractional coordinates in $Ca_9Fe(PO_4)_7$ (22) as initial parameters for the refinement of the $Ca_9In(PO_4)_7$ at room temperature (we will call this modification β-$Ca_9In(PO_4)_7$). Atomic and anomalous scattering factors for Ca^{2+}, In^{3+}, P and O^- were taken from the International Tables, Vol. C (30). The split pseudo-Voigt function of Toraya (31) was fit to each profile, and the 11th-order Legendre polynomial to the background. The preferred orientation was corrected with the March–Dollase function on the assumption of a (001) cleavage plane.

In the structure of β-$Ca_9Fe(PO_4)_7$, Fe^{3+} cations occupy the $M5$ site of the β-$Ca_3(PO_4)_2$ structure. Calcium cations occupy the $M1$–$M3$ sites, while the $M4$ and $M6$ sites are vacant. The occupancy factor for the $M1$, $M2$ and $M3$ sites by Ca^{2+} cations and the $M5$ site by In^{3+} cations was allowed to be refined but did not deviate significantly from full occupation. The occupation of the $M4$ site of the

whitlockite-type structure was fixed at 0 as it was found in $Ca_9Fe(PO_4)_7$ (22).

After the last refinement, there was a good agreement between the observed and calculated patterns and reasonable values of isotropic temperature factors were found for all atoms. Final plots of the observed electron density maps did not show residual peaks. The electron density on different electron density maps [$\Delta\rho_{exp.}(xyz)$] was within $\pm 0.8\ \bar{e}\text{Å}^{-3}$. The electron density maps were calculated using the GSAS program (32). The details of data collection and refinements are given in Table 1. The final atomic parameters are listed in Table 2. Table 3 presents selected interatomic distances. A part of the Rietveld profiles for $Ca_9In(PO_4)_7$ is shown in Fig. 1.

3.3. Electron Diffraction (ED) and High-Resolution Electron Microscopy (HREM)

The room temperature [0001]*, [10$\bar{1}$0]*, [$\bar{1}$101]* and [11$\bar{2}$0]* ED patterns for $Ca_9In(PO_4)_7$ are shown in Fig. 2. The diffraction patterns can be completely indexed in the $R3c$ space group using the unit-cell parameters determined by X-ray powder diffraction. The reflections in the [0001]* diffraction pattern obey the extinction condition ($-h + k = 3n$), imposed by the $R3c$ space group. The [10$\bar{1}$0]* zone pattern exhibits 000l, $l = 3n$, n-odd reflections forbidden by the $R3c$ symmetry. The intensity of these reflections, however, is systematically lower than the intensity of 000l, $l = 3n$ with n-even. On tilting the specimen around the (000l) axis the reflections with $l = 3n$, n-odd further weaken and vanish. The appearance of these forbidden reflections has been attributed to double diffraction. The 000l, $l = 3n$, n-odd reflections are absent in the [11$\bar{2}$0]* zone since the conditions for double diffraction in this zone are not present. The [11$\bar{2}$0]* diffraction pattern exhibits a rhombohedral shift of the spot rows along c* over $h \times 1/3\,c$*.

An HREM study has been performed along the [0001] and [10$\bar{1}$0] directions where the structure can be interpreted in terms of cation and oxygen columns. The contrast interpretation has been carried out by comparing the experimental images with the calculated ones. The positional parameters obtained from the X-ray powder refinement were taken as an input to simulate the HREM images.

Figure 3 shows an HREM image of $Ca_9In(PO_4)_7$ along the [0001] zone. The brighter dots in the HREM image are found to correspond to the indium atom columns while the less bright dots represent calcium. The calculated images for different defocus values and thicknesses show a good agreement with different parts of the experimental image. One of them for defocus ($\Delta f = -80$ nm) and thickness ($t = 1$ nm) is given as an inset.

A [10$\bar{1}$0] HREM image is shown in Fig. 4. A detailed examination of different areas and grains only revealed a single phase (space group $R3c$) in contrast to $Ca_9Fe(PO_4)_7$ where $R3m$ (or $R3$) structure microdomains were found to be present inside the $R3c$ matrix (24). Apparently, the formation of $R3m$ (or $R3$) microdomains inside the $R3c$ whitlockite-type $Ca_9R(PO_4)_7$ phase is the result of a changing composition (R^{3+} cations partially occupy the $M5$ site).

TABLE 1
Crystallographic Data, Recording Conditions, and Refinement Results for Different Modifications of $Ca_9In(PO_4)_7$

	β-	β'-
Temperature, K	297	973
Space group	$R3c$	$R\bar{3}c$
2Θ range(°)	10–110	10–110
Step scan increment (2Θ)	0.01	0.02
I_{max}	42 0921	59 357
Unit-cell parameters:		
a (Å),	10.4008(1)	10.4611(2)
c (Å),	37.272(1)	37.874(1)
V (Å^3),	3491.7(1)	3589.4(1)
Z	6	6
Number of reflections	496	1018
Reliable factors	4.69; 3.54	4.27; 3.16
R_{WP}, R_P		
R_I, R_F	1.81; 0.84	4.11; 2.51
S	1.80	3.12

4. PHASE TRANSITIONS IN $Ca_9In(PO_4)_7$

4.1. Second-Harmonic Generation (SHG)

Figure 5 shows the thermal dependence of the second harmonic for a powder sample of $Ca_9In(PO_4)_7$. A clear decrease of the SHG signal is observed when heating in the range 870–910 K. During subsequent cooling the SHG signal reappears.

Disappearance of the SHG signal on heating and its reappearance with definite thermal hysteresis on cooling is in accordance with the first-order polar-to-centrosymmetric phase transition which has previously been observed in $Ca_9Fe(PO_4)_7$ (24). A noticeable difference in the value of the SHG signal before ($I^+ = 1.32$) and after ($I^- = 0.87$) the heating–cooling cycle may be explained by the thermal history of the polycrystalline sample with a variable domain microstructure. Curve 1 in Fig. 5 represents the temperature dependence of the SHG signal for $Ca_9In(PO_4)_7$ powder quenched from 973 K to room temperature. The SHG investigations have shown that a reversible phase transition $\beta \leftrightarrow \beta'$ takes place for $Ca_9In(PO_4)_7$ over the temperature range 890–910 K. At temperatures higher than the temperature of the phase transition this compound crystallizes into a centrosymmetrical space group.

TABLE 2
Fractional Atomic Coordinates and Thermal Parameters for Different Modifications of $Ca_9In(PO_4)_7$

Atom		Site	x	y	Z	B_{iso}[a]	Occup.
Ca1	β-	18*b*	0.7198(3)	0.8533(3)	0.4317(1)	0.35(5)	1
	β′-	36*f*	0.7078(3)	0.8532(9)	0.4334(1)	3.15(8)	1
Ca2	β-	18*b*	0.6215(2)	0.8244(4)	0.2320(1)	0.27(5)	1
	β′-						
Ca3	β-	18*b*	0.1309(3)	0.2771(2)	0.3258(1)	0.30(4)	1
	β′-	36*f*	0.524(3)	0.477(3)	0.0051(2)	3.3(2)	0.5
In	β-	6*a*	0.0	0.0	0.0	0.36(2)	1
	β′-	6*b*	0.0	0.0	0.0	2.44(8)	1
P1	β-	6*a*	0.0	0.0	0.2690(1)	0.44(8)	1
	β′-	12*c*	0.0	0.0	0.2631(3)	2.9(4)	0.5
P2	β-	18*b*	0.6850(3)	0.8550(4)	0.1346(1)	0.10(8)	1
	β′-	36*f*	0.6469(4)	0.831(1)	0.0315(1)	2.8(1)	1
P3	β-	18*b*	0.6536(4)	0.8454(5)	0.0314(1)	0.54(8)	1
	β′-						
O11	β-	6*a*	0.0	0.0	0.3108(2)	0.10(8)	1
	β′-	12*c*	0.0	0.0	0.3054(7)	4.5(6)	0.5
O12	β-	18*b*	0.0179(7)	0.8662(5)	0.2549(2)	0.10(8)	1
	β′-	36*f*	0.128(2)	0.017(3)	0.2382(5)	4.5(8)	0.5
O21	β-	18*b*	0.7266(7)	0.9088(6)	0.1745(2)	0.10(9)	1
	β′-	36*f*	0.7314(7)	0.851(2)	0.1735(2)	3.1(1)	1
O22	β-	18*b*	0.755(1)	0.7701(9)	0.1197(2)	0.10(9)	1
	β′-	36*f*	0.749(2)	0.761(2)	0.1200(5)	3.1(1)	1
O23	β-	18*b*	0.7307(9)	0.0034(7)	0.1119(2)	0.10(9)	1
	β′-	36*f*	0.733(2)	0.000(2)	0.1166(6)	3.1(1)	1
O24	β-	18*b*	0.5108(7)	0.764(1)	0.1291(2)	0.10(9)	1
	β′-	36*f*	0.5212(7)	0.761(4)	0.1274(1)	3.1(1)	1
O31	β-	18*b*	0.6063(8)	0.9531(8)	0.0446(2)	0.10(9)	1
O32	β-	18*b*	0.5813(9)	0.6920(9)	0.0499(2)	0.10(9)	1
O33	β-	18*b*	0.8261(8)	0.920(1)	0.0400(2)	0.10(9)	1
O34	β-	18*b*	0.6314(5)	0.8223(9)	0.9908(1)	0.10(9)	1

[a] B_{iso}(O) refined for all oxygen atoms in each or all of kind P(1–3)O_4 tetrahedron.

4.2. Dielectric and Conductivity Measurements

The dielectric constant for $Ca_9In(PO_4)_7$ (Fig. 6a, b) demonstrates a ferroelectric-type maximum at $T_c^+ = 902$ K on heating (Fig. 6a, b) and $T_c^+ = 880$ K on cooling (Fig. 6b) irrespective of the frequency of the electric field applied. The less distinct maximum seen on tan $\delta(T)$ curve (Fig. 6c) just below T_c is also characteristic of a ferroelectric phase transition, reflecting the usual enhancement of the domain wall mobility at the temperature border of existence of the ferroelectric phase.

The ferroelectric phase transition in $Ca_9In(PO_4)_7$ is accompanied by a sharp rise of the electrical conductivity (Fig. 6d). A jump in the temperature dependence of the conductivity was observed on both heating and cooling, with a temperature hysteresis exactly the same as in SHG and dielectric constant investigations. The good reproducibility of the $\sigma(T)$ behavior in the "heating–cooling" cycle served as an indicator of the quasi-equilibrium conditions for the specimen during the measurements.

Figure 7 shows a typical DSC curve for $Ca_9In(PO_4)_7$ obtained at a heating rate of 5 K/min. The endothermic effect is well marked. The enthalpy of the transition is 4.62 J/g. The shape of the DSC curve for $Ca_9In(PO_4)_7$ indicates a first-order phase transition $T_c = 902$ K.

4.3. X-Ray Powder Diffraction

Figure 8 shows the temperature dependence of the X-ray powder patterns of $Ca_9In(PO_4)_7$. The patterns are all similar but the intensity of the Bragg reflections with $h\,k\,l$ ($l \neq 2n$) decreases when increasing the temperature from 293 K to 1273 K. The phase transition is accompanied by a jump in the temperature dependence of the a and c lattice parameters (Table 4, Fig. 9).

4.4. Electron Diffraction (ED)

Heating the sample from 293 to 1193 K does not introduce significant changes in the ED patterns. This means that only a phase transition from an $R3c$ to a $R\bar{3}c$ symmetry is possible because the $R3c$ and $R\bar{3}c$ space groups have identical reflection conditions.

TABLE 3
Interatomic Distances (Å) for Different Modifications of $Ca_9In(PO_4)_7$

Distance	β–	Distance	β′–
Ca1–O12	2.446(6)	Ca1–O12	2.51(2)
–O22	2.798(9)	–O12A	2.53(2)
–O23	2.553(9)	–O21	2.464(7)
–O24	2.45(1)	–O22	2.49(2)
–O24A	2.53(1)	–O22A	2.78(2)
–O31	2.456(8)	–O23	2.55(2)
–O32	2.316(8)	–O24	2.54(3)
–O34	2.342(5)	–O24A	2.55(3)
<Ca–O>	2.49	<Ca–O>	2.55
Ca2–O12	2.261(6)		
–O21	2.366(7)		
–O22	2.420(8)		
–O23	2.315(7)		
–O31	2.607(8)		
–O32	2.679(8)		
–O33	2.45(1)		
–O33A	2.46(1)		
<Ca–O>	2.44		
Ca3–O11	2.559(2)	Ca3–O11	2.73(1)
–O12	2.952(7)	–O12	2.94(2)
–O21	2.668(6)	–O21	2.39(3)
–O22	2.506(8)	–O21A	2.65(3)
–O23	2.429(7)	–O21B	2.95(3)
–O31	2.415(8)	–O21C	3.25(3)
–O32	2.574(8)	–O22	2.44(2)
–O34	2.583(8)	–O22A	2.45(3)
–O34A	2.612(7)	–O23	2.52(3)
<Ca–O>	2.59	–O23A	2.43(3)
		Ca3–Ca3A	0.95(1)
In–O24 × 3	2.128(8)	In–O24 × 6	2.260(6)
–O33 × 3	2.164(8)		
P1–O11	1.560(9)	P1–O11	1.60(3)
–O12 × 3	1.584(5)	–O12 × 3	1.57(1)
<P1–O>	1.58	<P1–O>	1.58
		P1–P1A	0.99(3)
		O12–O12A	0.95(4)
P2 –O21	1.572(8)	P2–O21	1.527(8)
–O22	1.502(7)	–O22	1.50(2)
–O23	1.609(7)	–O23	1.56(2)
–O24	1.583(6)	–O24	1.527(7)
<P2–O>	1.57	<P2–O>	1.53
P3 –O31	1.513(8)		
–O32	1.545(8)		
–O33	1.590(6)		
–O34	1.532(6)		
<P3–O>	1.55		

4.5. Structure of the β′-phase

The structural data for β-$Ca_9In(PO_4)_7$ at room temperature were used as the starting model for the structure refinement at 973 K. Because of the close similarity of this new high-temperature phase to the whitlockite-type β-$Ca_3(PO_4)_2$, it may be referred to as β′-$Ca_9In(PO_4)_7$ in contrast with the low-temperature β-$Ca_9In(PO_4)_7$. The atomic coordinates of β-$Ca_9In(PO_4)_7$ were transformed to the space group $R\bar{3}c$ ($a_{\beta'} \approx a_\beta$; $b_{\beta'} \approx b_\beta$; $c_{\beta'} \approx c_\beta$). In this model, the Ca1 and Ca2 sites, $P2O_4$ and $P3O_4$ tetrahedra of the whitlockite-type structure are equivalent, while the In, Ca3 and P1 sites are situated at the center of symmetry.

After refinement of this model, the thermal parameter for calcium cation in Ca3 (site symmetry 18*d*) was $B_{iso.} = 7.3(2)$. A displacement of Ca3 from the special position at the center of symmetry ($\frac{1}{2}$,0, 0) leading to a half-occupied general position gave $B_{iso.} = 3.1(2)$. The $P2O_4$ tetrahedra were localized quite easily, but difficulties appeared in the localization of the P1 and O12 atoms in the $P1O_4$ tetrahedra. The thermal parameter for the P1 position (site 6*a*) was $B_{iso.} = 9.5(8)$. A displacement of the phosphorus atoms in the P1 site from the special position in the pseudocenter of symmetry (0, 0, $\frac{1}{4}$) to a half-occupied special position (site 12*c*) gave $B_{iso.} = 2.7(4)$. In the β-$Ca_3(PO_4)_2$ structure O11 and O12 oxygen atoms lie on the threefold axis and on a plane perpendicular to this axis, respectively. The displacement of the O12 oxygen atoms from the special position (x, $\bar{x}$, z) leading to a half-occupied general position gave $B_{iso.} = 4.5(2)$.

After this last refinement, there was a good agreement between the observed and calculated patterns and reasonable values of the isotropic temperature factors were found for all atoms. The details of data collection and refinements are given in Table 1. The final atomic parameters are listed in Table 2. Table 3 presents selected interatomic distances. A portion of the Rietveld profiles for β′-$Ca_9In(PO_4)_7$ is shown in Fig. 10.

5. DISCUSSION

The compound $Ca_9In(PO_4)_7$ in both the β- and β′-modifications is isostructural to the natural mineral whitlockite (11) and to β-$Ca_3(PO_4)_2$ (10). However, $M_3(PO_4)_2$ phosphates of divalent elements with a larger radius (M = Sr, Ba, Pb) (33, 34) are known to crystallize in the $K_2Pb(SO_4)_2$ or palmierite structure (35).

The palmierite- and whitlockite-type structures are very similar and are made up of isolated PO_4^{3-} tetrahedra, which connect the MO_n polyhedra into a 3-D framework via common vertices. Figure 11 shows the [11$\bar{2}$0] projections of the whitlockite-type (β-$Ca_3(PO_4)_2$ (a); β- (b) and β′-$Ca_9In(PO_4)_7$ (c)) and palmierite-type ($Sr_3(PO_4)_2$ (d)) structures. Along the *c*-axis in these structures it is possible to differentiate two types of columns: *A* and *B*. In the *B*-type column, three MO_n polyhedra and two tetrahedra PO_4^{3-} alternate. The *A*-type column consists of a sequence of polyhedra and cavities.

All layers in the palmierite-type structure are built up by *B* columns (Fig. 11d). Sr^{2+} cations occupy two crystallographically different positions and *B* columns can be presented as [$\cdots$–$M2O_{10}$–$M1O_{12}$–$M2O_{10}$–PO_4–PO_4–$\cdots$]. The β-$Ca_3(PO_4)_2$ structure consists of two different layers. One of them is built only by *B* columns (Fig. 11a), the

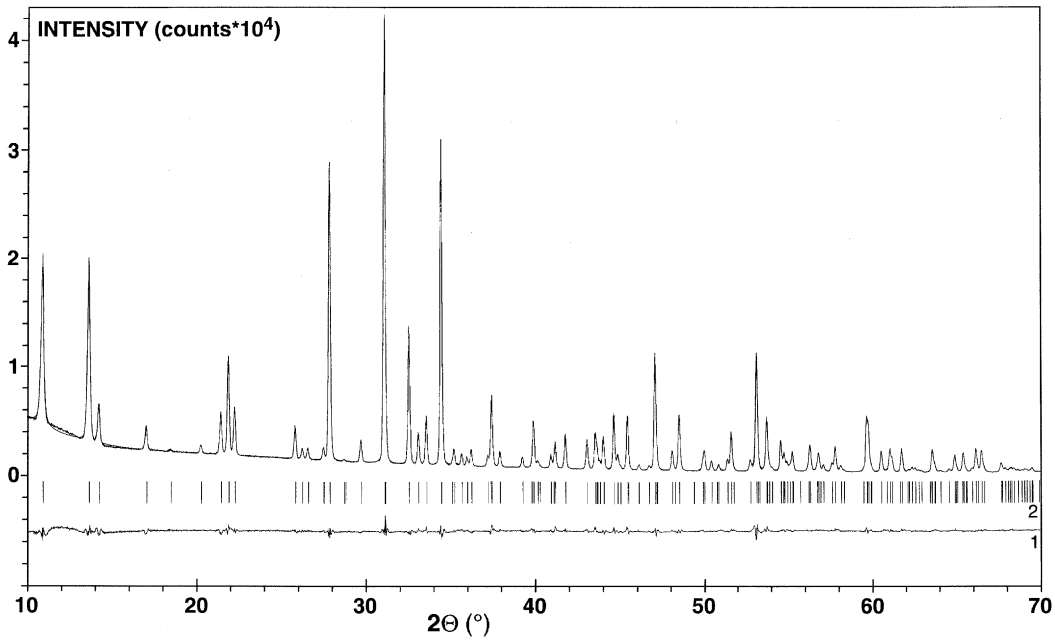

FIG. 1. Portion of the Rietveld refinement profiles for β-$Ca_9In(PO_4)_7$: (1) difference XRD pattern and (2) Bragg reflections.

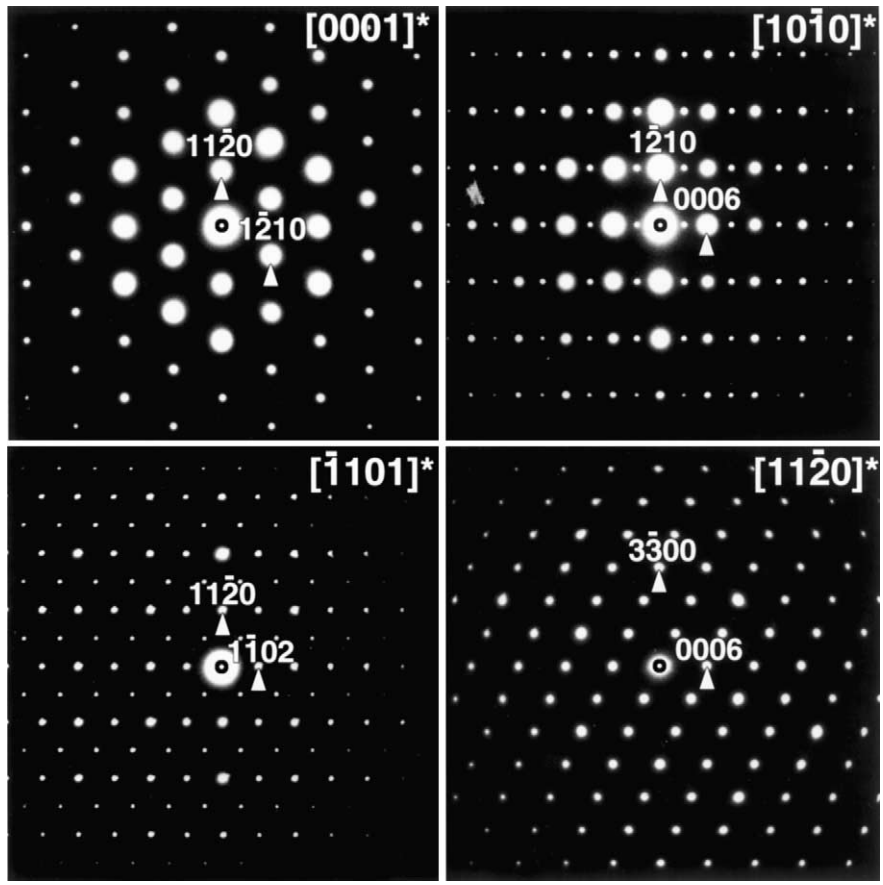

FIG. 2. Electron diffraction patterns along the main zone axes for $Ca_9In(PO_4)_7$ at room temperature.

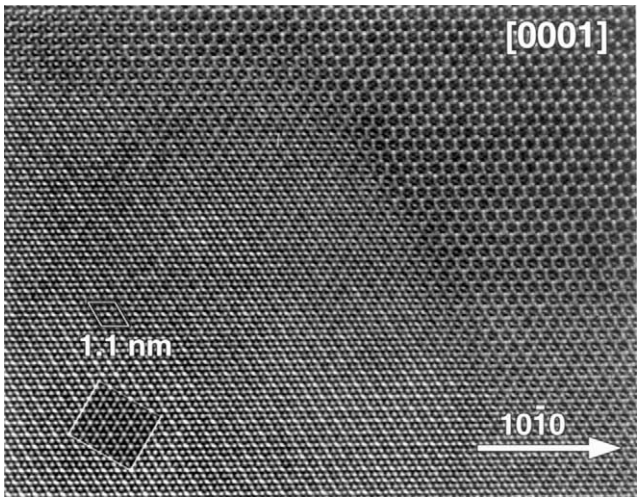

FIG. 3. High-resolution electron microscopy image for $Ca_9In(PO_4)_7$ along the [0001] zone. The calculated image for defocus ($\Delta f = -80$ nm) and thickness ($t = 1$ nm) model is shown as an inset.

second one by columns *A* and *B* (Fig. 11b). A rotation of the PO_4^{3-} tetrahedra leads to a change in coordination of the cation polyhedra in comparison with the palmierite-type structure. The *B* and *A* columns in the whitlockite-type structure can be presented as [$\cdots$–*M*1O_8–*M*3O_8–*M*2O_8–PO_4–PO_4–$\cdots$] and [...–PO_4–*M*4O_{15}–*M*5O_6–M6O_{10}–$\cdots$], respectively. In the β-$Ca_3(PO_4)_2$ structure, the *M*4 site in *A* columns is half-occupied while the *M*6

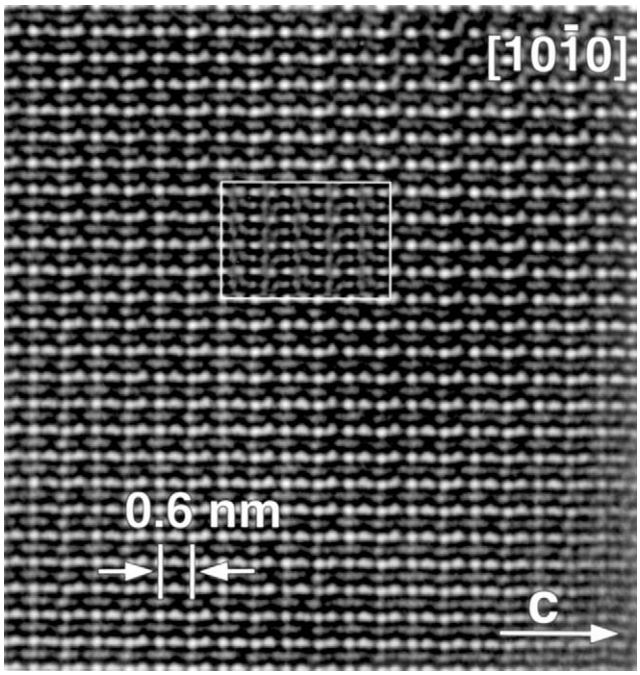

FIG. 4. High-resolution electron microscopy image for $Ca_9In(PO_4)_7$ along the [10$\bar{1}$0] zone. The calculated image ($\Delta f = -80$ nm and $t = 10$ nm) is shown as an inset.

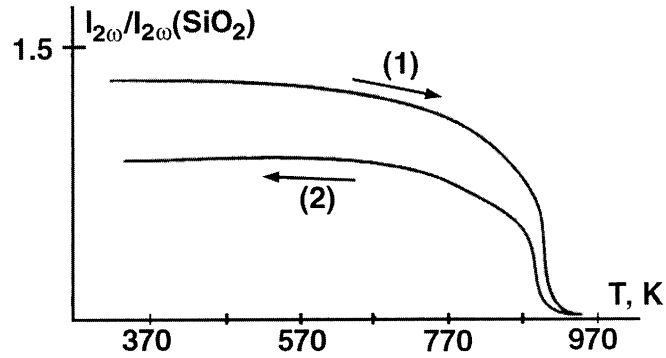

FIG. 5. Thermal dependencies of second-harmonic values for $Ca_9In(PO_4)_7$. (1) - heating, (2) – cooling.

site is vacant. The structure of β'-$Ca_9In(PO_4)_7$ is intermediate between the palmierite and the whitlockite structures (Fig. 12*c*).

In β- and β'-$Ca_9In(PO_4)_7$ cations occupy four crystallographical positions of the whitlockite-type structure. Cations Ca^{2+} and In^{3+} occupy *M*1–*M*3 and *M*5 positions of the whitlockite-type structure, respectively. The *M*4 and *M*6 sites of the whitlockite-type structure in $Ca_9In(PO_4)_7$ were found to be vacant.

The β- and β'-$Ca_9In(PO_4)_7$ structures are very similar. The main difference between them is the orientation of the $P1O_4$ tetrahedra. During the $\beta \leftrightarrow \beta'$ phase transition, half of the $P1O_4$ tetrahedra change orientation (Fig.12a–c). In the low-temperature modification there is one coordination polyhedron for the position Ca3. Each $Ca3O_8$ polyhedron shares its eight-oxo ligands with five tetrahedra and connects two $P1O_4$ tetrahedra (Fig. 12a). Only O11 and O12 atoms of one $P1O_4$ are shared with $Ca3O_8$. The atoms O11A and O12A of another $P1O_4$ tetrahedron, located at 6.66 and 4.32 Å from Ca3 are not included into its coordination. In the high-temperature β'-modification, two polyhedra for calcium cations are formed in the Ca3 position. In one of these polyhedra two O11 atoms are turned in the direction of Ca3 (Fig. 12b) and located at 2.73 Å (O11A) and 3.67 Å (O11). Because of the displacement of the calcium cations from the center of symmetry, only one of the O11 atoms is included within the coordination sphere of Ca3 (Fig. 12b) and located at a distance of 2.73 Å. The Ca3–O12 and Ca3–O12A distances are 4.58 and 3.84 Å, accordingly. In the other Ca3 polyhedron O11 atoms are turned in the opposite direction (Fig. 12c). In this polyhedron only one O12A atom of the $P1O_4$ tetrahedron ($d_{Ca3–O12} = 2.94$ Å) is included into the coordination sphere of the second position of Ca3 (Fig. 12c). The second O12 atom of the $P1O_4$ tetrahedron is located at a distance of 3.73 Å. The Ca3–O11 and Ca3–O11A distances are 6.45 and 5.69 Å, respectively. Thus, in a centrosymmetric phase there are two polyhedra for calcium cations in the Ca3 position. As long as it was not possible

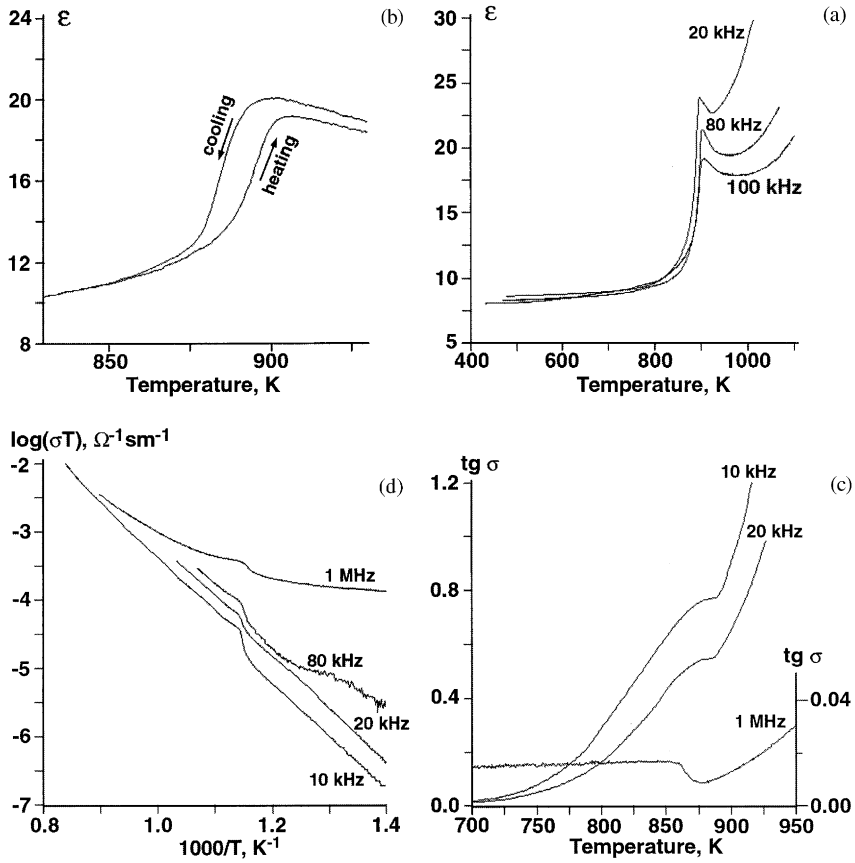

FIG. 6. Different temperature dependencies in $Ca_9In(PO_4)_7$: (a) the dielectric constant (ε) and (c) loss tangent (tan δ) at different frequencies on heating; (b) in details the temperature dependence of the dielectric constant (ε) at frequency 100 kHz; (d) conductivity (σ(T)) at different frequencies on heating.

to define the superstructure by X-ray powder diffraction and electron diffraction methods, the description was done in a subcell with an "effective" distance of $d_{Ca3–Ca3A}$ = 0.95 Å.

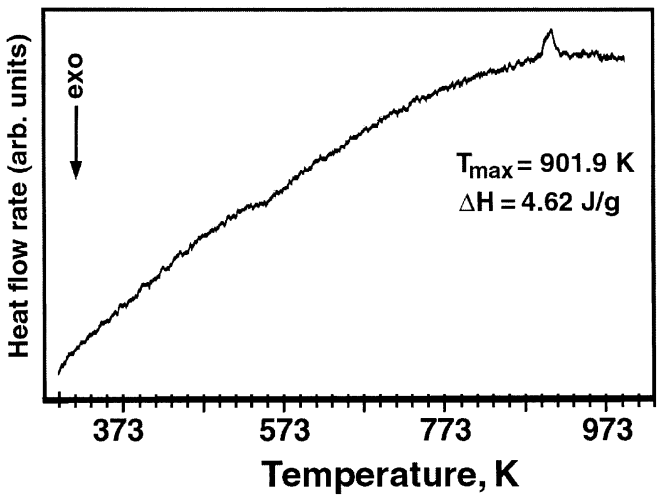

FIG. 7. DSC curve recorded between 293 and 1013 K for $Ca_9In(PO_4)_7$.

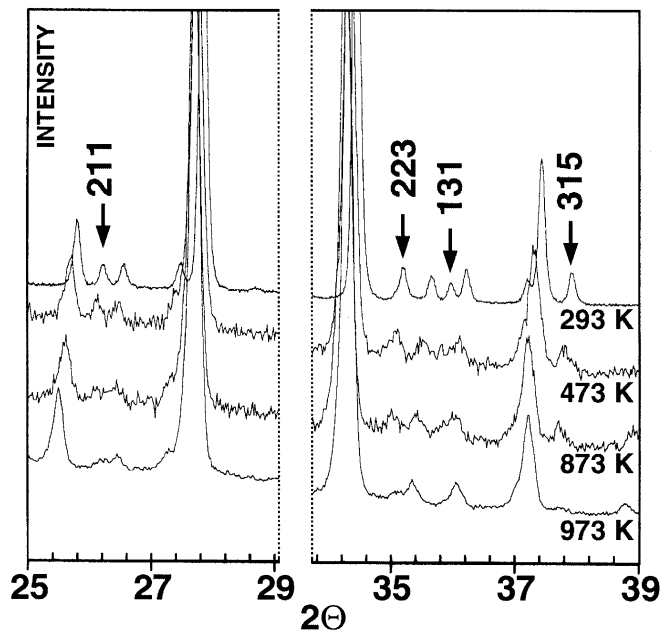

FIG. 8. Temperature dependence of X-ray patterns for $Ca_9In(PO_4)_7$. Reflections with odd *l* indexes in space group *R*3*c* are marked.

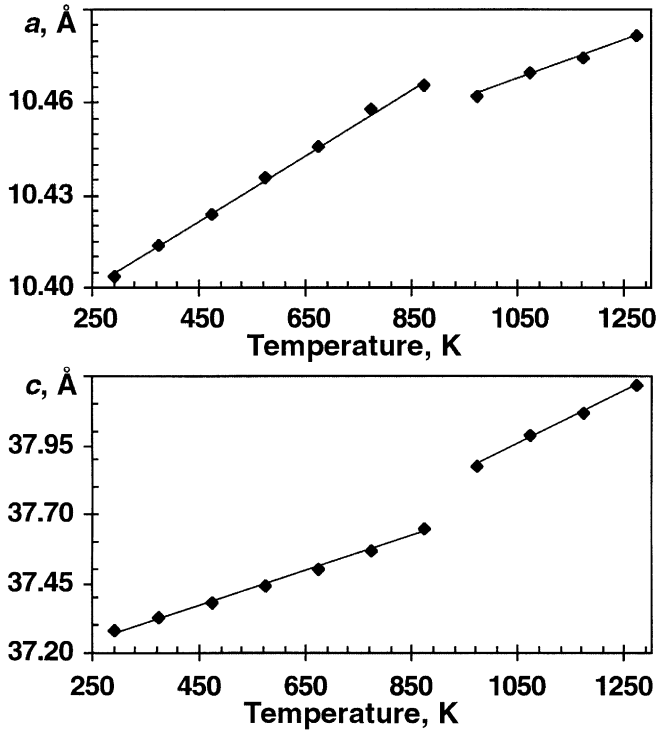

FIG. 9. Thermal dependence of the unit cell parameters a and c for $Ca_9In(PO_4)_7$.

TABLE 4
Unit Cell Parameters of Double Phosphate $Ca_9In(PO_4)_7$ at Different Temperatures

T, K	a, Å	c, Å	V, Å^3
297	10.4008(1)	37.275(1)	3492.0(3)
373	10.4138(8)	37.330(2)	3505.9(4)
473	10.4236(8)	37.379(2)	3517.2(5)
573	10.4357(9)	37.441(3)	3531.2(5)
673	10.4461(9)	37.497(3)	3543.5(6)
773	10.4577(9)	37.569(3)	3558.2(5)
873	10.4658(9)	37.644(3)	3570.8(5)
973	10.4618(2)	37.8756(4)	3590.1(7)
1073	10.4695(6)	37.9834(8)	3605.6(2)
1173	10.4745(6)	38.0698(8)	3617.2(2)
1273	10.4817(6)	38.1662(8)	3631.4(2)

In the structure β-$Ca_9In(PO_4)_7$ each O11 atom, located in a special position on the 3-fold axis is connected by three calcium atoms in the Ca3 position ($d_{Ca3–O11}$ = 2.559 Å). However, three equivalent Ca3–O11 bonds prevent a turn of the $P1O_4$ tetrahedra. We assume that the phase transition starts with the displacement of the calcium atoms in the Ca3 position and weakening of the Ca3–O11 bonds which enables a change of the $P1O_4$ tetrahedra orientation. In case of such reorientation the P1 atoms almost do not change their position. The other atoms of the structure are slightly displaced (0.05–0.25 Å) during the phase transition with the P2 and P3 tetrahedra only rotating slightly (Fig. 12b, c).

The SHG study in $Ca_9In(PO_4)_7$ indicates that the reversible ferroelectric $\beta \leftrightarrow \beta'$ phase transition ($R3c \leftrightarrow R\bar{3}c$) takes place at 902 K. The symmetry of the low-temperature phase must be related to the symmetry of the high-temperature phase by imposing a spontaneous polarization vector symmetry (36). This condition is fulfilled for the

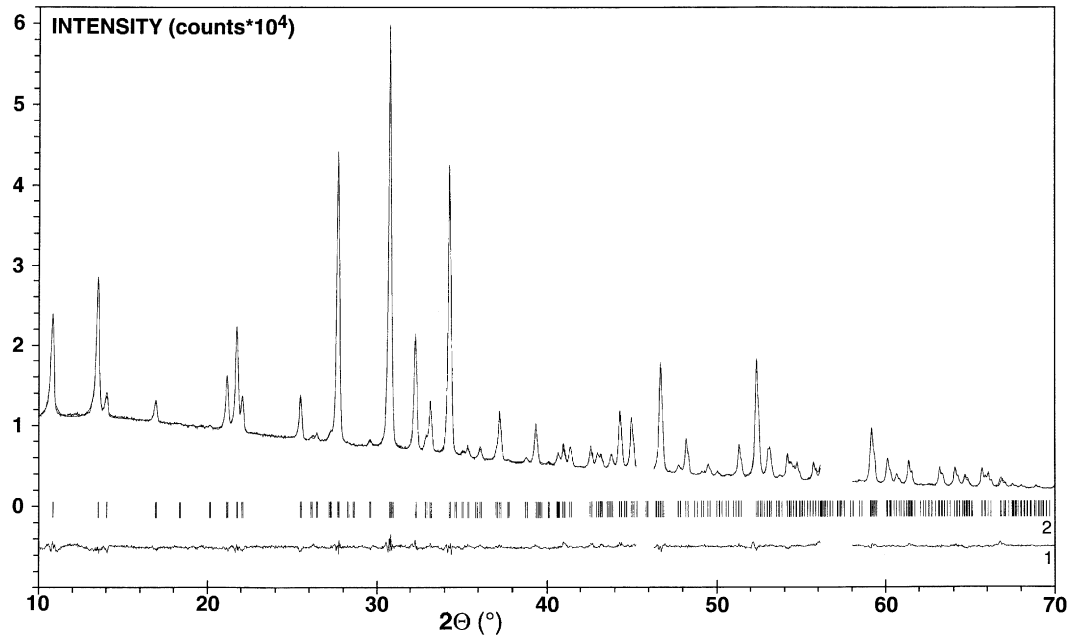

FIG. 10. Portion of the Rietveld refinement profiles for β'-$Ca_9In(PO_4)_7$: (1) difference XRD pattern and (2) Bragg reflections.

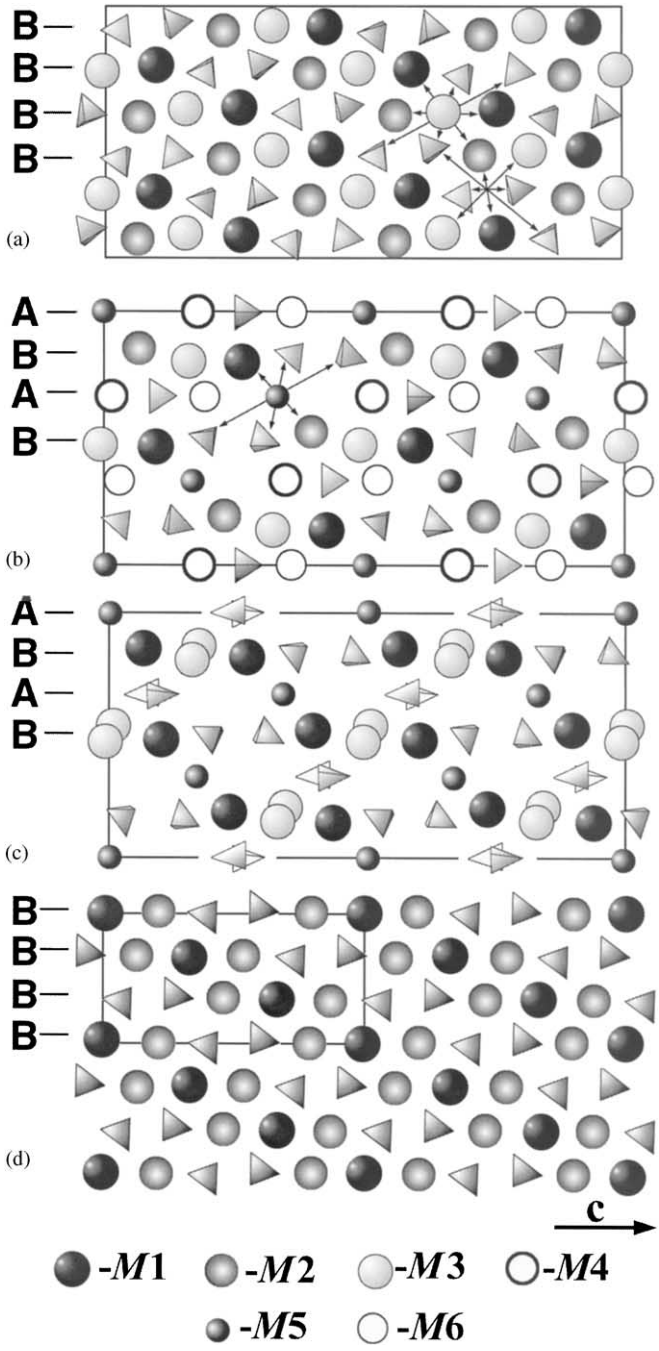

FIG. 11. Projections of the whitlockite- (a–c) and palmierite-type (d) structures along [11$\bar{2}$0]: layers with only *B* columns of β-$Ca_3(PO_4)_2$ (a) and $Sr_3(PO_4)_2$ (d); layers with *A* and *B* columns of β- (b) and β'-$Ca_9In(PO_4)_7$ (*c*). Arrows present elements of the structure connected by the pseudocenter of symmetry.

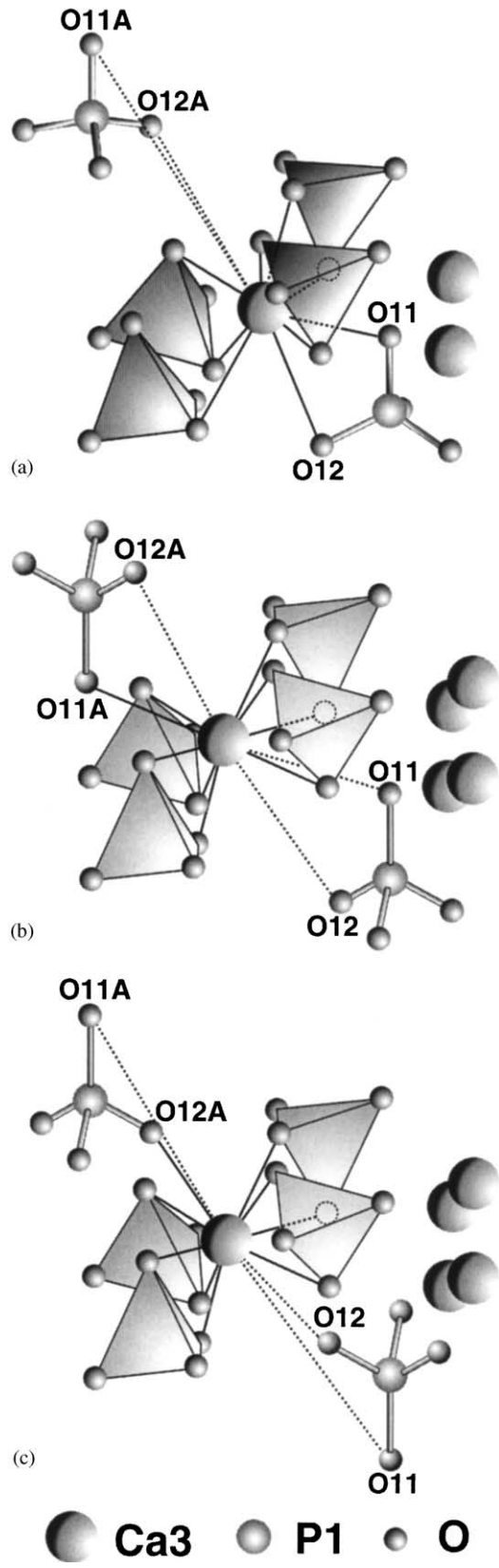

FIG. 12. Fragments of the structures β- (a) and β'-$Ca_9In(PO_4)_7$ (b, c) with Ca3 polyhedra.

phase transition in $Ca_9In(PO_4)_7$ with its symmetry changing from R3c to $R\bar{3}c$. Moreover, since the transformation does not affect the translation symmetry of the crystal, its unit cell does not change through the phase transition; this is also the case for $Ca_9In(PO_4)_7$. Together with the small

dielectric constant anomaly at T_c and the value P_s = 2–3 $\mu C/cm^2$ (estimated from SHG data), we have enough arguments to consider $Ca_9In(PO_4)_7$ as a new pseudo-proper ferroelectric with a high Curie temperature and a small spontaneous polarization.

The polar modification of β-$Ca_9In(PO_4)_7$ is stable at room temperature while the centrosymmetric modification is stable only at temperatures above the transition temperature (T_c = 902 K) and cannot be obtained by quenching to room temperature. For $Ca_9In(PO_4)_7$, a first order phase transition can be assumed from DSC, SHG and dielectric data. The phase transition in $Ca_9In(PO_4)_7$ is accompanied by changes in the orientation of half of the $P1O_4$ tetrahedra and calcium cation disordering in the *M*3 sites.

ACKNOWLEDGMENTS

This work was supported by the Russian Foundation for Basic Research (Grant 00-03-32660, 01-03-06121 and 01-03-06122). V.A. Morozov is grateful to DWTC (Belgium) for financial support. This work is performed within the framework of IUAP 4/10. O.I. Lebedev is on leave from the Institute of Crystallography, Russian Academy of Science, 117333 Moscow, Russia.

REFERENCES

1. M. Lind, S. Overgaard, H. Glerup, K. Søballe, and C. Bünger, *Biomaterials* **22,** 189 (2001).
2. S. Langstaff, M. Sayer, T. J. N. Smith, and S. M. Pugh, *Biomaterials* **22,** 135 (2001).
3. L. Clèries, J. M. Fernández-Pradas, and J. L. Morenza, *Biomaterials* **21,** 1861 (2000).
4. H. Monma and M. Goto, *J. Ceram. Soc. Jpn.* **91,** 473 (1983)
5. J. Ando, *Bull. Chem. Soc. Jpn.* **31,** 196 (1958).
6. S. Attali, M. Lenzi, and J. Lenzi, *Bull. Chem. Soc. France* **2–3,** 1135 (1981).
7. S. S. Romdhane and G. Bonel, *C. R. Acad. (France)* **294,** 245 (1982).
8. R. W. Nurse, J. H. Welch, and W. Gutt, *Nature* **182,** 1230 (1958).
9. R. W. Nurse, J. H. Welch, and W. Gutt, *J. Chem. Soc.* **220,** 1077 (1959).
10. L. Ruan, X. Wang, and L. Li, *Mat. Res. Bull.* **31,** 1207 (1996).
11. P. Roux, D. Louer, and G. Bonel, *C. R. Acad. Sci.* **286,** 549 (1978).
12. A. L. Mackay and D. P. Sinha, *J. Phys. Chem. Solids* **28,** 1337 (1967).
13. H. Koelmans, J. J. Engelsman, and R. S. Admiraal, *J. Phys. Chem. Solids* **11,** 172 (1959).
14. S. S. Romdhane, G. Bonel, and G. Bacquet, *Mater. Res. Bull.* **18,** 559 (1983).
15. J. S. O. Evans, J. Huang, and A. W. Sleight, *J. Solid State Chem.* **157,** 255 (2001).
16. V. A. Morozov, I. A. Presnyakov, A. A. Belik, S. S. Khasanov, and B. I. Lazoryak, *Crystallogr. Rep.* **42,** 758 (1997).
17. M. Mathew, L. W. Schroeder, B. Dickens, and W.E. Brown, *Acta Crystallogr. B* **33,** 1325 (1977).
18. B. I. Lazoryak, *Rus. Chem. Rev.* **65,** 287 (1996).
19. B. Dickens, L.W. Schroeder, and W.E. Brown, *J. Solid State Chem.* **10,** 232 (1974).
20. C. Calvo and R. Gopal, *Amer. Miner.* **60,** 120 (1975).
21. V. N. Golubev, B. N. Viting, O. B. Dogadin, B. I. Lazoryak, and R. G. Aziev, *Rus. J. Neorg. Chem.* **35,** 3037 (1990).
22. B. I. Lazoryak, V. A. Morozov, A. A. Belik, S. S. Khasanov, and S. Sh. Shekhtman, *J. Solid State Chem.* **122,** 15 (1996).
23. G. N. Kustova, E. N. Yurchenko, E. B. Burgina, M. M. Andrushkevich, and P. A. Buyanov, *Zh. Strukt. Khim.* **20,** 1019 (1979.)
24. B. I. Lazoryak, V. A. Morozov, A. A. Belik, S. Yu. Stefanovich, V. V. Grebenev, I. A. Leonidov, E. B. Mitberg, S. A. Davydov, O. I. Lebedev, and G. Van Tendeloo, *Chem. Mater.*, submitted.
25. A. A. Belik, F. Izumi, S. Yu. Stefanovich, A. P. Malakho, B. I. Lazoryak, I. A. Leonidov, O. N. Leonidova, and S. A. Davydov, *Chem. Mater*, submitted.
26. Powder Diffraction File, Card 45-338, JCPDS; International Center for Diffraction Data, 1601 Park Lane, Swarthmore, PA 19081.
27. S. Yu. Stefanovich, *in* "Proceedings of the European Conference on Lasers and Electro-Optics (CLEO-Europe'94)." Amsterdam, 1994, p. 249.
28. H. M. Rietveld, *Acta Crystallogr.* **22,** 151 (1967).
29. F. Izumi and T. Ikeda, *Mater. Sci. Forum* **321–324,** 198 (2000).
30. E. M. Maslen, A. G. Fox, and M. A. O'Keefe, "International Tables for Crystallography," Vol. C, pp. 500–502. Kluwer, Dordrecht, 1992.
31. H. Toraya, *J. Appl. Crystallogr.* **23,** 485 (1990).
32. A. C. Larson and R. B. Von Dreele, Generalized Crystal Structure Analysis System (GSAS). LAUR 86–748, Los Alamos, 1988, 150p.
33. W. H. Zachariasen, *Acta Crystallogr.* **1,** 263 (1948).
34. H. N. Ng and C. Calvo, *Can. J. Phys*, **53,** 42 (1975).
35. H.G. Bachmann and W. Kleber, *Fortsch. Mineral.* **31,** 9 (1952).
36. M. E. Lines and A. M. Glass. "Principles and Application of Ferroelectrics and Related Materials." Clarendon Press, Oxford 1977.